Isolating the Poroelastic Response of the Groundwater System in InSAR Data from the Central Valley of California

S. Kang[1] and R. Knight[1]

[1]Department of Geophysics, Stanford University.

Corresponding author: Seogi Kang (sgkang09@stanford.edu)

Key Points:

- Developed a new approach to isolate the poroelastic component in InSAR data by removing the hydrologic loading component.
- Provided the first detailed analysis of the loading response in InSAR data.
- Found that the loading response on average represents 62% of the deformation in InSAR measurements in the Central Valley.

Abstract

Working with five years (2015-2019) of high quality interferometric synthetic aperture radar (InSAR) data covering the Central Valley of California, we developed a new approach to isolate the poroelastic component in InSAR data by estimating and removing the hydrologic loading component. K-means clustering was used to identify the InSAR deformation time-series dominated by the loading response and those dominated by the poroelastic response. The former time-series include seasonal oscillations of uplift and subsidence primarily related to mass changes in snow and ice in the adjacent mountain range, while the latter include interannual deformation and seasonal oscillations related to changing head in the valley. The loading component accounts for, on average, 62% of the deformation in the Central Valley. Without correcting for the loading response, the deformation due to the poroelastic response (and therefore any derived estimate of change in head) is underestimated by 50-60% in areas of the valley.

Plain Language Summary

In the Central Valley of California, changes in ground elevation, often referred to as surface deformation, are mainly due to the changes in groundwater head, which result in a poroelastic response, and the changes in mass of water, snow, and ice, which result in a hydrologic loading response. Interferometric synthetic aperture radar (InSAR) provides a powerful way to map this surface deformation with an unprecedented level of resolution in space and time. The close connection between the InSAR data and changes in head has created great interest in using the InSAR data for mapping and monitoring changes in groundwater head, information that is of critical importance for groundwater management. However, without the removal of the loading response in the InSAR data, derived changes in head from the InSAR data can include significant errors that could impact decisions for groundwater management. Working with the five years of publicly available InSAR data in the Central Valley, we developed a new approach that can remove the loading component thereby advancing the ability to use InSAR data to monitor changes in groundwater head.

1 Introduction

Interferometric synthetic aperture radar (InSAR) (Farr & Liu, 2014; Zebker et al., 1994) provides a powerful way to map the deformation of the ground surface. Deformation quantified with InSAR data has been used to monitor the poroelastic response of groundwater systems caused by changes in effective stress that are driven by changes in hydraulic head due to the removal or addition of groundwater (Castellazzi et al., 2016; Miller et al., 2017; Smith & Knight, 2019). This introduces the potential use of InSAR data to remotely monitor the changes in hydraulic

head. But it cannot be assumed that the deformation captured in the InSAR data is solely due to a poroelastic response. It has been recognized that the deformation of the ground surface is also sensitive to the loading caused by mass changes in liquid water, ice, and/or snow in the hydrologic system (Argus et al., 2014; Borsa et al., 2014). Therefore, in order to use the InSAR technique to monitor the poroelastic response of the groundwater system, the loading portion of the measured surface deformation needs to be accounted for. The high quality InSAR data now available have made it possible to do this. Working with five years of InSAR data (2015-2019) and hydrologic data from the data-rich Central Valley of California, U.S.A., we developed a new approach that removes the deformation due to the loading response in the InSAR data so as to isolate the deformation due to the poroelastic response. This significantly advances our ability to use InSAR data to monitor changes in hydraulic head, information that is of critical importance for groundwater management.

The groundwater system of the Central Valley, the location of which is shown in Figure 1, is composed of sediments sourced from the Sierra Nevada and the Coast Ranges. Interbedded clays account for ~65% of the system (Faunt, 2010). In the southern part of the valley, there is a regional confining unit, the Corcoran Clay, which separates the shallow unconfined aquifer from the deeper confined aquifer; its extent is shown in Figure 1. The interbedded clays, which are orders of magnitude more compressible than coarser-grained materials, are responsible for much of the observed poroelastic response and associated deformation in areas where there are large head changes (Ireland et al., 1982). The months between November 1st and April 1st are defined as the wet season and other months as the dry season (Faunt, 2010) with the head typically reaching a maximum near the end of the wet season and a minimum near the end of the dry season.

The starting point for our study were earlier publications that provide a detailed analysis of the deformation, captured in InSAR data, associated with the poroelastic response in the Central Valley and the deformation, captured in Global Positioning System (GPS) data, associated with the loading response in the Central Valley and adjacent mountain range. Descriptions of both refer to interannual deformation, which is defined as uplift or subsidence that continues uninterrupted for more than one year, and seasonal deformation, which is defined as alternating periods of uplift and subsidence temporally correlated with the seasons.

Studies of the poroelastic response (Farr and Liu, 2014; Levy et al., 2020; Neely et al., 2021; Lees et al., 2022) have focused on the link between the deformation of the ground surface and changes in head in the underlying groundwater system. The key observations of direct relevance to this study are summarized here. Seasonal cycles of subsidence and uplift have been found to correlate with seasonal oscillations in head, with subsidence when head falls and uplift when head rises; this is the elastic deformation response. When head in the interbedded clays falls below the historic minimum, significant subsidence of the ground surface occurs; this is due to an increase in the compressibility of the clays and the resulting inelastic, i.e., permanent or irreversible, compaction. A component of this form of subsidence can be delayed for decades

due to the residual compaction in the clays that can continue long after cessation of the groundwater pumping that causes the head drop in the surrounding, coarser-grained materials. In the San Joaquin Valley, the southern part of the Central Valley, there have been many observations of periods of interannual subsidence, but few observations of periods of interannual uplift.

The studies by Argus et al. (2014, 2017) provide the framework that we adopted for studying deformation associated with the loading response in the time period of our study, 2015 – 2019. Major sources of the seasonal loading response in the Central Valley were identified to be changes in the mass of snow and ice in the mountain range, the Sierra Nevada, along the eastern edge of the valley, the mass of water held as soil moisture in the valley, the mass of water in the reservoirs in the valley and Sierra Nevada, and the mass of groundwater in the valley. Of these sources, changes in snow and ice in the Sierra Nevada dominate the loading response observed regionally. The magnitude of deformation of the ground surface due to a change in mass loading will be proportional to the change in mass, and slowly decay from the location of the mass change (e.g., $1/r$ for loading at the surface) (Farrell, 1972). This response to loading suggests that the spatial variation of the loading response in the valley will be very smooth. The deformation associated with the loading response was found to display a seasonal character that oscillates out-of-phase with the changes in the mass of the snow/ice in the Sierra Nevada with peaks around April 1st and troughs around October 1st (Argus et al., 2014). A model of the continued removal of groundwater over multiple years predicts interannual uplift during our study period of about 1-2 mm/year in the southern part of valley where there has been chronic over-pumping of groundwater and much less, <0.5 mm/year, in the northern part of the valley (Argus et al., 2017). Interannual subsidence due to loading has not been reported or predicted during our study period, and is highly unlikely given the severe droughts at that time.

The ability to use InSAR data to remotely monitor changes in head requires that the component of the deformation associated with the poroelastic response be isolated. Given the various sources that can cause a loading response, it is very likely that deformation due to loading will be present in the InSAR data at all locations in the Central Valley. Therefore, misinterpretation of the InSAR data in terms of the variation in head would result if a loading response were neglected and deformation attributed solely to a poroelastic response. To address this issue, we developed a new approach that first estimates the loading response at all locations throughout the Central Valley and then uses that to isolate the poroelastic response in the InSAR data. This enables the use of InSAR data to remotely monitor changes in head.

2 Data Sources and Preparation

The InSAR data used in this study were processed by TRE ALTIMERA (TREA) and provided to the California Department of Water Resources to support the implementation of the Sustainable Groundwater Management Act, passed by the California Legislature in 2014. The data are time-series of vertical deformation from 1st January 2015 to 19th September 2019 with measurements

every 7 days, resulting in 284 time channels. The level of error in the InSAR data, which was estimated by comparison with GPS data from 181 stations, is ± 9 mm (TREA, 2021). Within the valley, there are about 1.7M InSAR data locations. In order to obtain a regular distribution of data, we gridded the data with a uniform cell size of 0.01 degree (approximately 1 km×1 km) then, in each cell, used the last time channel in the InSAR data to find the location where the deformation corresponded to the median value within the cell; the InSAR time-series at this location were used as the data for this cell. This gridding of the data reduced the number of data locations and time-series to 50,472.

Figure 1 shows the gridded InSAR data, displaying the total subsidence from 1st January 2015 to 19th September 2019 with data missing in only ~5% of the valley. Most of the large subsidence anomalies, within the 5 cm subsidence contours, fall inside the lateral extent of the Corcoran Clay, which indicates the importance of this confining clay layer for generating conditions that lead to subsidence.

Snow water equivalent (SWE) data covering the Sierra Nevada were available over the time period October 2009 to October 2019 (Schneider & Molotch, 2016). These data, monthly averages of daily measurements, provided SWE in units of mass of water per unit area and were in a gridded format with a cell size of approximately 500 m × 500 m. The spatial integral of all the data for each month was calculated allowing us to obtain a single SWE time-series, corresponding to the time period of the InSAR data, representing the total mass change of the snow and ice in the Sierra Nevada.

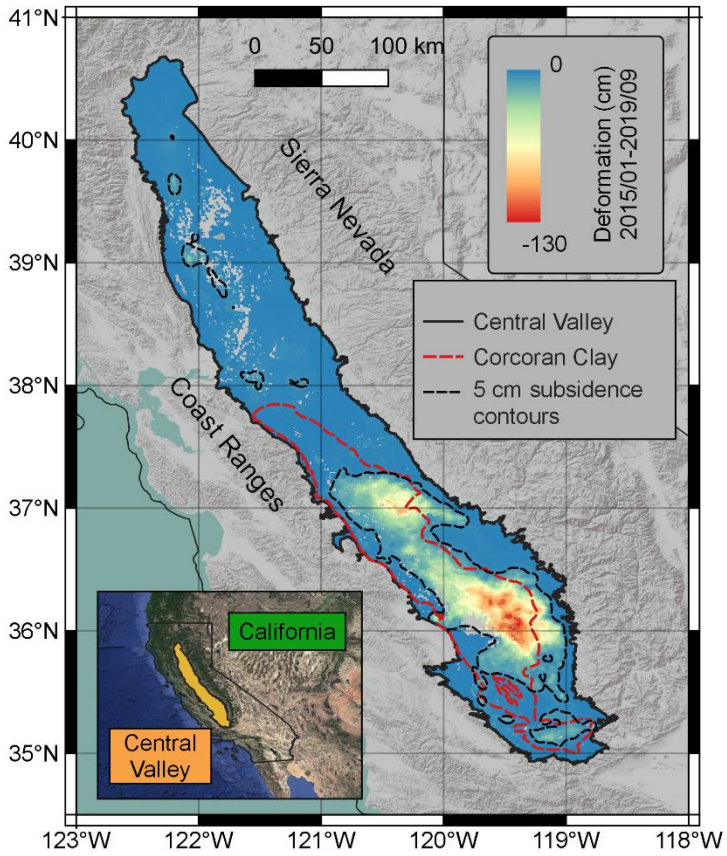

Figure 1. 2D map of deformation derived from InSAR data in the Central Valley of California, USA, for the time period 1st January 2015 to 19th September 2019.

4 Methods of Data Analysis

We began with the assumption that there are two major components of the InSAR deformation data, d, in the Central Valley: the deformation data corresponding to the poroelastic response, referred to as the poroelastic data, $d_{\text{poroelastic}}$, and the deformation data corresponding to the loading response, referred to as the loading data, d_{loading}. This is represented by the following equation

$$d(x, y; t) = d_{\text{poroelastic}} + d_{\text{loading}} + \text{noise} \quad (1)$$

where are x and y are spatial co-ordinates, and t is the time channel of the InSAR data. Example sources of noise are residual tectonic motion and atmospheric phase delays with the level of noise generally smaller than the error level of $\pm$ 9 mm in the InSAR-measured deformation (Argus et al., 2017). Given that the interannual uplift due to loading was estimated to be much less than the error level, and that interannual subsidence due to loading was highly unlikely, we presumed that the loading data would appear as the seasonal oscillations described by Argus et al. (2014), with peaks around October 1st and troughs around April 1st. The poroelastic data were

expected to display a combination of interannual subsidence or uplift, and seasonal oscillations that were out-of-phase with the loading data. Our objective was to estimate the loading data in the InSAR deformation data and remove it so as to isolate the poroelastic data.

4.1 Isolating the poroelastic data

As a way to estimate the loading data at all locations in the Central Valley, we first identified areas where the InSAR data were dominated by the loading data, with some relatively minor contribution from poroelastic data. We did this using K-means clustering (Lloyd, 1982) to classify the InSAR time-series into clusters, each of which has distinct temporal features. In any cluster where the loading data dominate the InSAR data we expected to see evidence of the seasonal oscillations described by Argus et al. (2014).

The starting InSAR time-series $d(t)$ contains measured surface deformation every 7 days where $d(t)$ represents cumulative surface deformation from 1st January 2015 to the time channel, *t*. This integrating process decreases the noise level but acts as a low-pass filter damping high-frequency content. Taking the difference between $d(t)$ and $d(t + \Delta t)$ results in the surface deformation over the time between two time channels, Δt. Reducing Δt improves the high-frequency content but also increases the noise level. Hence, there is a trade-off in selecting the optimal Δt.

We implemented a Python-based machine learning package, Scikit-learn (Pedregosa et al., 2011), for the K-means clustering. Two parameters that needed to be selected were n_{cluster} and Δt. The optimal values of n_{cluster}= 6 and Δt = 35 days were determined through an iterative process with the goal of maximizing the number of clusters while maintaining sufficient dissimilarity between the clusters. The latter was done by minimizing the variance of the time-series included in each cluster.

After clustering, we identified one cluster (referred to as Cluster 1) where the loading data – seen as the seasonal oscillation described by Angus et al. (2014) – dominated the InSAR data. Within this cluster, we took each of the InSAR time series and removed any interannual trend due to interannual deformation (subsidence or uplift) which we attributed to a poroelastic response. We assumed that the interannual trend was piece-wise linear for each year, so set up a piece-wise linear interpolation problem, used a least squares approach to calculate the annual deformation rate, and subtracted it from each InSAR time-series to obtain a detrended time-series. The set of detrended time-series was taken to represent the loading data which dominated the deformation data at all the locations included in Cluster 1. At all other locations, the InSAR data were either a more balanced combination of loading data and poroelastic data or dominated by poroelastic data.

In order to subtract the loading data from all of the InSAR time-series which contained variable levels of loading and poroelastic data, we needed to mathematically describe the loading data at all locations in the valley. We presumed that the loading response would be present everywhere and would vary smoothly, so treated it as an unknown regional response represented as a smooth 2D surface defined by polynomials. For estimating this response, we adapted a technique widely used for the removal of regional effects in the processing of potential field data (Li & Oldenburg, 1998). This required reducing the dimensionality of the InSAR time-series using principal

component analysis (PCA). PCA was applied to the detrended InSAR data from Cluster 1, resulting in ten principal components and scores for each principal component (PC). The first PC displayed the seasonal variation interpreted as the loading response with peaks towards the end of the dry season and troughs towards the end of the wet season (inset of Figure 2a), so was selected as representative of the loading response. We fitted a surface (shown in Figure 2b) to the scores of the first PC (shown in Figure 2a) using 4^{th}-degree polynomials with an iterative process that maximized the fit while penalizing the artifacts. We projected the fitted surface onto all InSAR data locations and then applied inverse PCA to obtain the estimated loading data. This gave us the final estimated loading data for all InSAR locations in the valley. Scikit-learn (Pedregosa et al., 2011) was used for conducting the PCA. For the polynomial fitting, a Python-based spatial processing package, Verde (Uieda, 2018), was used.

The estimated loading data were subtracted from the InSAR data, at all locations, resulting in the data that we interpreted to be solely the poroelastic data. At each InSAR data location we calculated the percentage of the total InSAR data that corresponded to loading data.

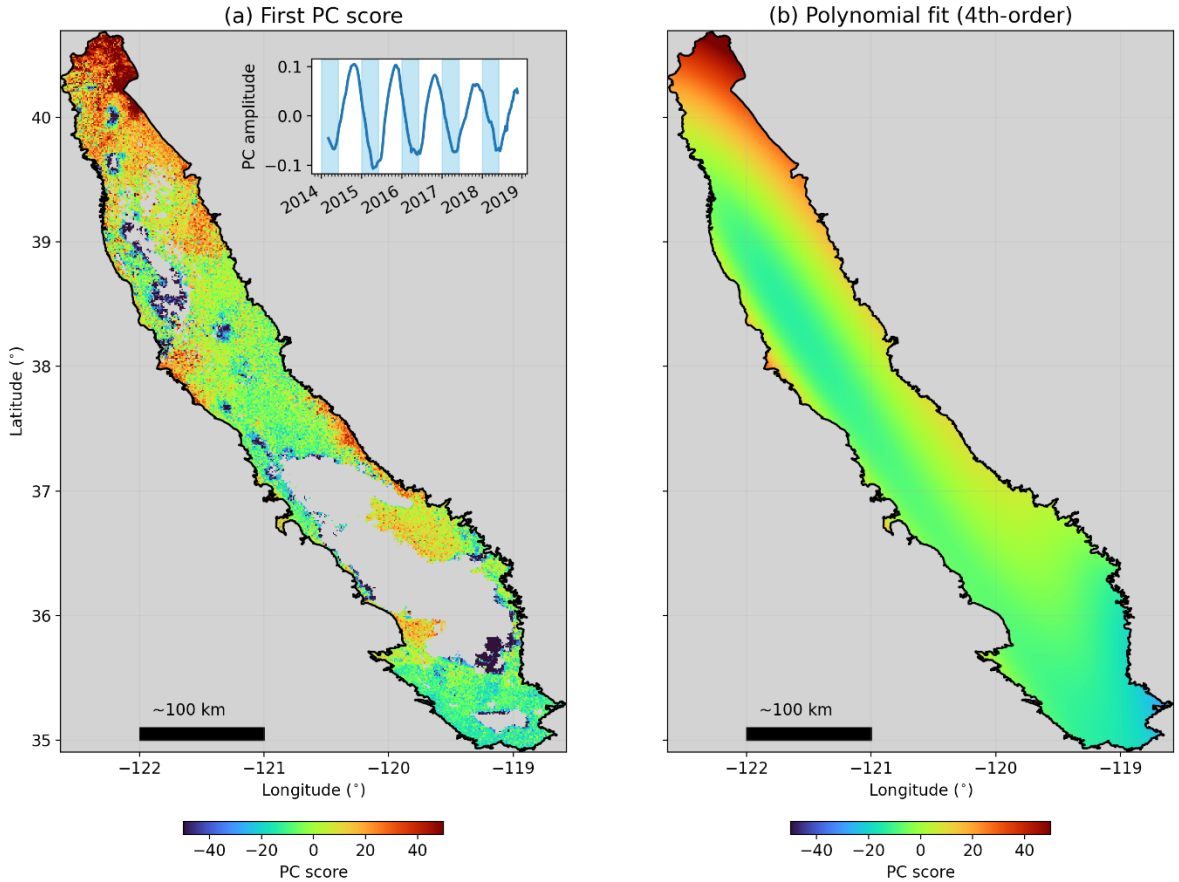

Figure 2. (a) First principal component (PC) score on a 2D map. Inset shows the first PC as a time-series. (b) Estimated 2D surface of the first PC score using 4^{th} order polynomial fitting. Black line shows the boundary of the Central Valley. Gray regions within the valley indicate either no available InSAR data or locations of Clusters 2-5.

5 Results and Discussion

5.1 K-means clustering

In Figure 3a, we show the locations of the InSAR times-series falling into the six clusters obtained through the K-means clustering; we also show the 5-cm subsidence contours of the InSAR data at the last time channel from Figure 1. Although there were no spatial constraints imposed for the clustering, the clusters clearly aggregate into distinct regions of the Central Valley revealing data-driven spatial patterns. In Figure 3b, we show the mean InSAR time-series for each of the six clusters.

Seventy-six percent of all InSAR time-series were classified as Cluster 1, which corresponds to approximately 72% of the area of the valley. The mean InSAR time-series from this cluster corresponds to what we would expect to see in a region where the deformation data are dominated by loading data – seasonal oscillations with peaks towards the end of the dry season and troughs towards the end of the wet season, with minor interannual subsidence due to a poroelastic response. The mean time-series in Cluster 1 also shows higher frequency oscillations, most likely associated with sub-seasonal changes in the loading response.

The InSAR time-series that are classified in Clusters 2 to 6 fall primarily within the 5-cm subsidence contours, with most located in the southern part of the valley where large a poroelastic response has been observed (e.g., Neely et al., 2021; Smith et al., 2017). These time-series are dominated by the poroelastic response as evidenced by the presence of interannual subsidence and seasonal oscillations that are out-of-phase with the loading response, i.e., uplift in the wet season and subsidence in the dry season. The mean time-series in Clusters 2, 3, and 4 show the interannual subsidence while those of Clusters 5 and 6 show pronounced seasonal oscillations. The rate of interannual subsidence varies across the clusters with an average rate of 4 cm/year for Cluster 2, 10 cm/year for Cluster 3, 20 cm/year for Cluster 4, 1 cm/year for Cluster 5, and 8 cm/year for Cluster 6. The uplift in Cluster 5 during 2017 can be attributed to an increase in delivered surface water that decreased the need for, and thus the pumping of, groundwater.

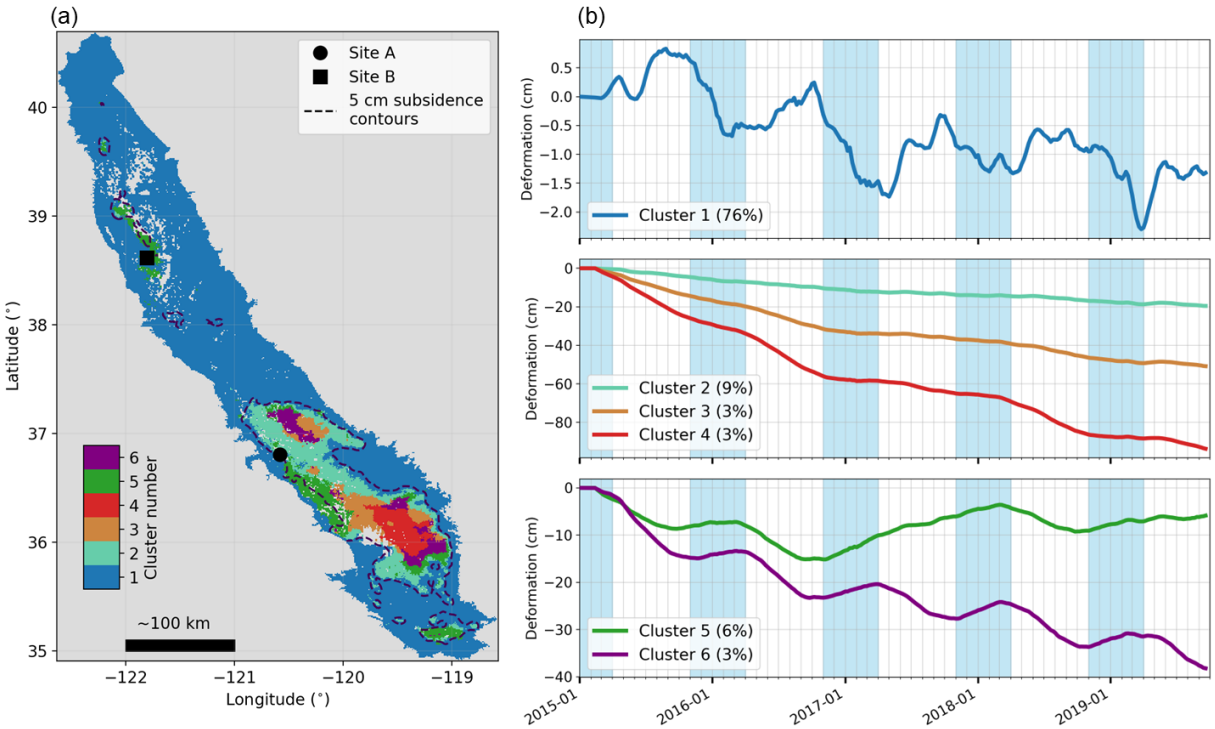

Figure 3. (a) Map displaying the locations of the six clusters resulting from K-means clustering of the InSAR data. Gray regions are either outside of the Central Valley or have no available InSAR data. (b) Mean InSAR time-series for each of the six clusters. Blue and white bars show the wet (1st November-1st April) and dry (the rest of the year) seasons, respectively.

5.2 The loading response

This is the first detailed study the loading response in InSAR data. Most analyses to date have focused exclusively on interpretation of InSAR data in terms of the poroelastic response. We first defined the loading data and then corrected for this in the InSAR data so as to obtain the data of primary interest for groundwater management – the data due to a poroelastic response related to head.

Our first step was to solve for the loading data at all locations in the Central Valley where InSAR data were available. Figure 4a shows the comparison of the mean time-series of the final estimated loading data in the valley and the total SWE time-series for the Sierra Nevada. We see the expected out-of-phase correlation between the two time-series where the presence of the snow or ice causes subsidence.

In Figure 4b, we show the percentage of the InSAR data that corresponds to loading data. The percentage is 62% over the entire valley. The loading data are on average 80% of the Cluster 1 InSAR data, which are dominated by the loading response. In the clusters dominated by the poroelastic response, the InSAR data in Clusters 2 and 5 contain a higher percentage of loading data - 6% and 12% respectively, than the data in Clusters 3 and 6 at 1%, and Cluster 4 at 0.7%.

These results demonstrate the importance, particularly in some parts of the valley, of first subtracting the loading data from the InSAR data in order to use the remaining data – the poroelastic data, to monitor changes in head. Given the large percentage of loading in the InSAR data in Cluster 1, an assumption that the InSAR data are reflecting purely a poroelastic response related to head would be invalid; and changes in head derived directly from the InSAR data in Cluster 1 would be highly inaccurate. In other clusters, where the percentage of loading is smaller than for those in Cluster 1, accounting for the loading response, will result in a more accurate representation of the poroelastic component, and thus a more accurate interpretation of changes in head.

We demonstrate the importance of correcting for the loading response by using examples from two sites – Site A and Site B, the locations of which are shown in Figures 3a and 4b. Site A is located close to the interface between Cluster 1 and 2. Site B is located close to the interface between Cluster 1 and 5. Comparisons of the time-series for the total InSAR data, the loading data, and the poroelastic data are shown in Figures 4c (for Site A) and 4d (for Site B). The most significant difference in terms of using InSAR data to monitor changes in head, is the amplitude of the peaks and troughs in the time series. Because the loading data are out of phase with the poroelastic data, the peaks and troughs in the poroelastic data are, in most cases, of higher amplitude that those in the total InSAR time series. Given that amplitude is linearly related to the change in head and change in groundwater storage, neglecting to correct for the loading data would result in underestimation of head and storage changes. The red arrows in Figures 4c and 4d show locations in the time-series where use of the total InSAR data would result an underestimation of head or storage change up to 50-60%.

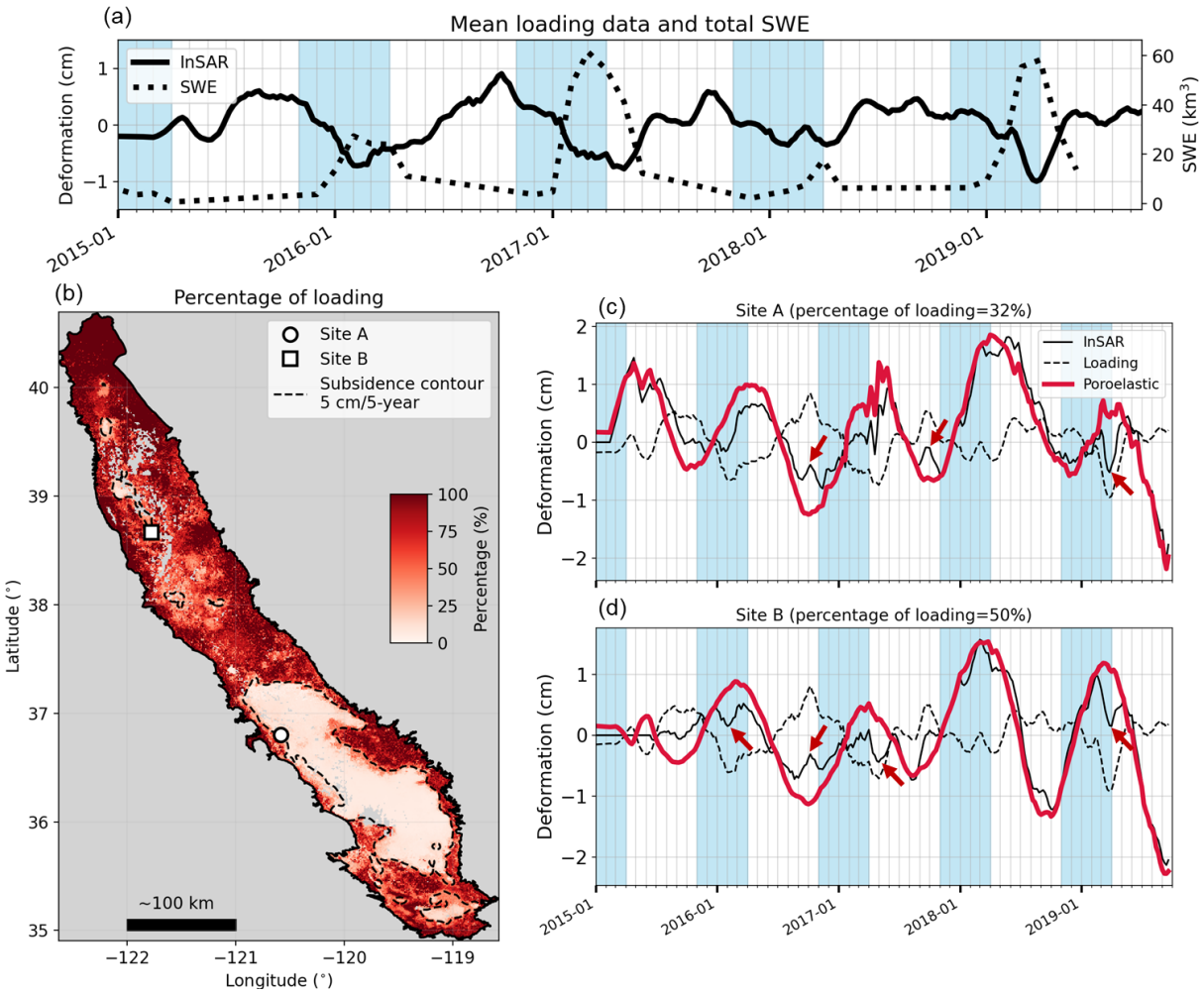

Figure 4. (a) Comparison of the mean time-series of the loading data and the total SWE time-series. (b) Percentage of the InSAR data that corresponds to loading data. Comparison of InSAR time-series, poroelastic data, and loading data at (c) Site A and (d) Site B; locations of the sites are shown in Figure 4b. Red arrows show examples where the use of the total InSAR data would introduce errors in the estimation of change in head or storage.

7 Conclusions

There is great interest in the use of InSAR data as a means of mapping and monitoring head changes in groundwater systems. In order to be used in this way, the component of the InSAR deformation data that is related to head changes – the poroelastic data – needs to be isolated.

The quantity and quality of InSAR data now available made it possible for us to develop a methodology to correct for the impact of loading on the InSAR deformation data, by subtracting the loading data from the total InSAR data. We conclude that this methodology, that corrects for the loading response, should be implemented whenever there is a desire to monitor changes in the groundwater system in the Central Valley with InSAR data. While we found that the percentage of the total InSAR data that the loading data comprise varies from 0.7% to 80%, the low percentages were found in areas with large total deformation, so are significant in terms of the deformation they represent. If the total InSAR deformation data are used to estimate head and storage changes instead of the poroelastic deformation data, there can be a high level of inaccuracy in the derived estimates. Our results suggest errors on the order of 50% to 60% in areas of the Central Valley.

As part of our methodology, we have derived from the InSAR data a quantitative description of the deformation throughout the Central Valley due to the mass loading with snow and ice in the Sierra Nevada. Beyond the importance of the use of this in isolating the poroelastic deformation data, there is the potential to integrate this loading response with other measurements of SWE so as to obtain improved accuracy in monitoring the spatial and temporal variation in SWE.

The methodology that we have developed employs numerical tools that are publicly available. It is thus readily transferrable to other areas in a similar hydrologic setting when there is a desire to use InSAR data to estimate head changes. In addition, the basic idea of using K-means clustering to classify InSAR time-series, could be utilized whenever there is a need to separate the various mechanisms contributing to an InSAR deformation measurement. The developed methodology can be adopted to support and advance the many ways in which InSAR data can be used for a wide range of applications in the Earth sciences.

Acknowledgments

We thank Matt Lees and Wesley Neely from Stanford Environmental Geophysics Research Group for helpful discussion about the physics of deformation mapped with InSAR data. Funding for this research was provided to R. Knight from the Gordon and Betty Moore Foundation (grant no. GBMF6189) and the NASA Applied Sciences Water Resources Program (award no. 80NSSC19K1248)..

Open Research

Data sets used in this research are publicly available through the open data portal of the California Department of Water Resources: https://data.cnra.ca.gov/dataset/tre-altamira-insar-subsidence.

References

Argus, D. F., Fu, Y., & Landerer, F. W. (2014). Seasonal variation in total water storage in California inferred from GPS observations of vertical land motion. *Geophysical Research Letters*, *41*(6), 1971–1980. https://doi.org/https://doi.org/10.1002/2014GL059570

Argus, D. F., Landerer, F. W., Wiese, D. N., Martens, H. R., Fu, Y., Famiglietti, J. S., et al. (2017). Sustained Water Loss in California's Mountain Ranges During Severe Drought From 2012 to 2015 Inferred From GPS. *Journal of Geophysical Research: Solid Earth*, *122*(12), 10,559-10,585. https://doi.org/10.1002/2017JB014424

Borsa, A. A., Agnew, D. C., & Cayan, D. R. (2014). Ongoing drought-induced uplift in the western United States. *Science*, *345*(6204), 1587–1590. https://doi.org/10.1126/science.1260279

Castellazzi, P., Martel, R., Rivera, A., Huang, J., Pavlic, G., Calderhead, A. I., et al. (2016). Groundwater depletion in Central Mexico: Use of GRACE and InSAR to support water resources management. *Water Resources Research*, *52*(8), 5985–6003. https://doi.org/https://doi.org/10.1002/2015WR018211

Chen, J., Knight, R., Zebker, H. A., & Schreüder, W. A. (2016). Confined aquifer head measurements and storage properties in the San Luis Valley, Colorado, from spaceborne InSAR observations. *Water Resources Research*, *52*(5), 3623–3636. https://doi.org/https://doi.org/10.1002/2015WR018466

Farr, T. G., & Liu, Z. (2014, November 3). Monitoring Subsidence Associated with Groundwater Dynamics in the Central Valley of California Using Interferometric Radar. *Remote Sensing of the Terrestrial Water Cycle*. https://doi.org/https://doi.org/10.1002/9781118872086.ch24

Farrell, W. E. (1972). Deformation of the Earth by surface loads. *Reviews of Geophysics*, *10*(3), 761–797. https://doi.org/https://doi.org/10.1029/RG010i003p00761

Faunt, C. C. (2010). *Groundwater availability of the Central Valley aquifer, California*. *US Geological Survey*.

Ireland, R. L., Poland, J. F., & Riley, F. S. (1982). *Land subsidence in the San Joaquin Valley, California, as of 1980*. *Open-File Report*. https://doi.org/10.3133/ofr82370

Lees, M., Knight, R., & Smith, R. (2022). Development and Application of a 1D Compaction Model to Understand 65 Years of Subsidence in the San Joaquin Valley. *Water Resources Research*, *58*(6), e2021WR031390. https://doi.org/https://doi.org/10.1029/2021WR031390

Li, Y., & Oldenburg, D. W. (1998). Separation of regional and residual magnetic field data. *GEOPHYSICS*, *63*(2), 431–439. https://doi.org/10.1190/1.1444343

Lloyd, S. (1982). Least squares quantization in PCM. *IEEE Transactions on Information Theory*, *28*(2), 129–137. https://doi.org/10.1109/TIT.1982.1056489

Miller, M. M., Shirzaei, M., & Argus, D. (2017). Aquifer Mechanical Properties and Decelerated Compaction in Tucson, Arizona. *Journal of Geophysical Research: Solid Earth*, *122*(10), 8402–8416. https://doi.org/https://doi.org/10.1002/2017JB014531

Neely, W. R., Borsa, A. A., Burney, J. A., Levy, M. C., Silverii, F., & Sneed, M. (2021). Characterization of Groundwater Recharge and Flow in California's San Joaquin Valley From InSAR-Observed Surface Deformation. *Water Resources Research*, *57*(4), e2020WR028451. https://doi.org/https://doi.org/10.1029/2020WR028451

Pedregosa, F., Varoquaux, G., Gramfort, A., Michel, V., Thirion, B., Grisel, O., et al. (2011). Scikit-learn: Machine Learning in {P}ython. *Journal of Machine Learning Research*, *12*, 2825–2830.

Schneider, D., & Molotch, N. P. (2016). Real-time estimation of snow water equivalent in the Upper Colorado River Basin using MODIS-based SWE Reconstructions and SNOTEL data. *Water Resources Research*, *52*(10), 7892–7910. https://doi.org/https://doi.org/10.1002/2016WR019067

Smith, R., & Knight, R. (2019). Modeling Land Subsidence Using InSAR and Airborne Electromagnetic Data. *Water Resources Research*, *55*(4), 2801–2819. https://doi.org/10.1029/2018WR024185

Smith, R., Knight, R., Chen, J., Reeves, J. A., Zebker, H. A., Farr, T., & Liu, Z. (2017). Estimating the permanent loss of groundwater storage in the southern San Joaquin Valley, California. *Water Resources Research*, *53*(3), 2133–2148. https://doi.org/https://doi.org/10.1002/2016WR019861

TREA. (2021). *InSAR Data Accuracy for California Groundwater Basins CGPS Data Comparative Analysis*. Retrieved from https://data.cnra.ca.gov/dataset/5e2d49e1-9ed0-425e-9f3e-2cda4a213c26/resource/a1949b59-2435-4e5d-bb29-7a8d432454f5/download/insar-data-accuracy-report-towill.pdf

Uieda, L. (2018). {Verde}: {Processing} and gridding spatial data using {Green's} functions. *Journal of Open Source Software*, *3*(29), 957. https://doi.org/10.21105/joss.00957

Zebker, H. A., Rosen, P. A., Goldstein, R. M., Gabriel, A., & Werner, C. L. (1994). On the derivation of coseismic displacement fields using differential radar interferometry: The Landers earthquake. *Journal of Geophysical Research: Solid Earth*, *99*(B10), 19617–19634. https://doi.org/https://doi.org/10.1029/94JB01179